NEURAL REGENERATION RESEARCH
www.nrronline.org

Research Article

Sodium selenite promotes neurological function recovery after spinal cord injury by inhibiting ferroptosis

https://doi.org/10.4103/1673-5374.339491
Date of submission: October 20, 2021
Date of decision: January 7, 2022
Date of acceptance: February 10, 2022
Date of web publication: April 29, 2022

Yi-Xin Chen[1, 2, 3, 4, 5, 6], Talifu Zuliyaer[1, 2, 3, 4, 5], Bin Liu[7], Shuang Guo[1, 2, 3, 4, 5], De-Gang Yang[1, 2, 3, 4, 5], Feng Gao[1, 2, 3, 4, 5, *], Yan Yu[2, 3, 5], Ming-Liang Yang[1, 2, 3, 4, 5], Liang-Jie Du[1, 2, 3, 4, 5], Jian-Jun Li[1, 2, 3, 4, 5, *]

From the Contents

Graphical Abstract *Sodium selenite is a potentially promising drug for spinal cord injury that inhibits ferroptosis.*

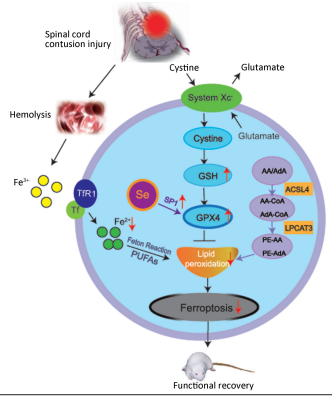

Abstract

Ferroptosis is a recently discovered form of iron-dependent cell death, which occurs during the pathological process of various central nervous system diseases or injuries, including secondary spinal cord injury. Selenium has been shown to promote neurological function recovery after cerebral hemorrhage by inhibiting ferroptosis. However, whether selenium can promote neurological function recovery after spinal cord injury as well as the underlying mechanism remain poorly understood. In this study, we injected sodium selenite (3 μL, 2.5 μM) into the injury site of a rat model of T10 vertebral contusion injury 10 minutes after spinal cord injury modeling. We found that sodium selenite treatment greatly decreased iron concentration and levels of the lipid peroxidation products malondialdehyde and 4-hydroxynonenal. Furthermore, sodium selenite increased the protein and mRNA expression of specificity protein 1 and glutathione peroxidase 4, promoted the survival of neurons and oligodendrocytes, inhibited the proliferation of astrocytes, and promoted the recovery of locomotive function of rats with spinal cord injury. These findings suggest that sodium selenite can improve the locomotive function of rats with spinal cord injury possibly through the inhibition of ferroptosis via the specificity protein 1/glutathione peroxidase 4 pathway.

Key Words: ferroptosis; glutathione peroxidase 4; glutathione; iron; lipid peroxidation; neural regeneration; secondary injury; sodium selenite; specificity protein 1; spinal cord injury

Introduction

Spinal cord injury (SCI) represents a severe form of trauma to the central nervous system and poses a serious threat to health in humans (No authors listed, 2016). The pathophysiology of SCI can be assigned to primary and secondary phases. Irreversible primary injury from mechanical forces leads to the compression or contusion of the spinal cord, while secondary injury occurs because of the development and perpetuation of the primary injury (Mourelo Fariña et al., 2017). The causes of secondary injury include ischemic edema, oxygen free radical production, calcium overload, inflammatory reactions, excitatory amino acid release, and necrosis or apoptosis initiation, which ultimately lead to loss of neural function. Thus, to treat primary SCI, it may be necessary to reduce or inhibit associated secondary injury.

In recent years, a new mode of cell death known as ferroptosis (Dixon et al., 2012) has been found to be involved in the pathological process of secondary injury associated with SCI (Shi et al., 2021). Ferroptosis is induced by intracellular iron overload and accumulation of lipid-derived reactive oxygen species (ROS). Compared with apoptosis, necrosis, and autophagy, ferroptosis has its own unique characteristics with regard to morphology, biochemistry, and genetic regulation (Dixon et al., 2012). The most important hallmarks of ferroptosis are the loss of capacity to repair lipid peroxides by glutathione peroxidase 4 (GPX4), oxidation of polyunsaturated fatty acid (PUFA)-containing phospholipids, and availability of redox-active iron (Dixon and Stockwell, 2019).

Currently, ferroptosis is considered to be triggered by iron overload followed by excessive generation of noxious lipid peroxides, which affect membrane permeability as well as integrity and eventually leads to cell damage (Hassannia et al., 2019). During these processes, lysophosphatidylcholine acyltransferase 3 (LPCAT3) and acyl-coenzyme A synthetase long-chain family member 4 (ACSL4) enable dense clustering of high-sensitivity PUFAs in cell membranes. Lipoxygenases, especially 15-lipoxygenase (Yang et al., 2016), oxidize PUFAs and generate intermediate products of lipid peroxidation known as lipid hydroperoxides, which include phosphatidylethanolamine-linked arachidonic acid or adrenic acid. These intermediate products accumulate within the plasma membrane and release ferroptosis signals (Wenzel et al., 2017). In the presence of Fe^{2+} within the cells, lipid hydroperoxides generate lipid-derived ROS, which cause irreversible cellular damage and death.

Previous studies have suggested that multiple pathways are involved in ferroptosis. In the GPX4 pathway, GPX4 is involved in conversion of toxic lipid

[1]School of Rehabilitation Medicine, Capital Medical University, Beijing, China; [2]China Rehabilitation Science Institute, Beijing, China; [3]Center of Neural Injury and Repair, Beijing Institute for Brain Disorders, Beijing, China; [4]Department of Spinal and Neural Functional Reconstruction, China Rehabilitation Research Center, Beijing, China; [5]Beijing Key Laboratory of Neural Injury and Rehabilitation, Beijing, China; [6]Department of Rehabilitation Medicine, Xiangya Hospital of Central South University, Changsha, Hunan Province, China; [7]Department of Spine Surgery, Hunan Provincial People's Hospital (The First Affiliated Hospital of Hunan Normal University), Changsha, Hunan Province, China
***Correspondence to:** Jian-Jun Li, 13718331416@163.com; Feng Gao, PhD, gaofeng5960@126.com.
https://orcid.org/000-0003-2663-5971 (Jian-Jun Li); https://orcid.org/0000-0002-9525-8324 (Feng Gao)

Funding: *This study was supported by the National Natural Science Foundation of China, No. 81870979 (to JJL); the Scientific Research Foundation of China Rehabilitation Research Center, No. 2020-02 (to JJL); and the Natural Science Foundation of Changsha, No. kq2014285 (to YXC).*
How to cite this article: *Chen YX, Zuliyaer T, Liu B, Guo S, Yang DG, Gao F, Yu Y, Yang ML, Du LJ, Li JJ (2022) Sodium selenite promotes neurological function recovery after spinal cord injury by inhibiting ferroptosis. Neural Regen Res 17(12):2702-2709.*

hydroperoxides to non-toxic lipid alcohols, thus playing a negative regulatory role in ferroptosis (Conrad and Friedmann Angeli, 2015; Seibt et al., 2019). The mevalonate pathway (Warner et al., 2000), ferroptosis suppressor protein 1 pathway (Bersuker et al., 2019; Doll et al., 2019), and other pathways (Gao et al., 2013; Kwon et al., 2015; Xie et al., 2016) have also been shown to modulate ferroptosis. Selenium has recently been shown to elevate selenoprotein and GPX4 levels by facilitating the activation of transcription factor AP-2 gamma and specificity protein 1 (SP1) in an intracerebral hemorrhage (ICH) mouse model, thus promoting GPX4-mediated resistance to oxidative damage and suppressing ferroptosis (Alim et al., 2019).

Initial studies of ferroptosis focused on tumor cells (Dolma et al., 2003; Yang and Stockwell, 2008; Dixon et al., 2012), and research on the cause of cancer and the specific underlying molecular mechanisms effectively promoted targeted treatment of cancer. In recent years, ferroptosis has also been observed in acute central nervous system disorders, including stroke (Zille et al., 2017; Alim et al., 2019), brain trauma (Zhang et al., 2018; Kenny et al., 2019; Wu et al., 2019; Xie et al., 2019), and SCI (Zhang et al., 2018; Yao et al., 2019). Ferroptosis has a vital role in SCI and suppressing ferroptosis provides neuroprotection (Yao et al., 2019; Zhang et al., 2019; Wang et al., 2020; Zhou et al., 2020). However, the specific molecular mechanisms remain unclear.

Selenium replaces sulfur in cysteine and is incorporated as selenocysteine in selenoproteins. Among the 25 selenoproteins in humans, GPX4 is recognized as the most important and has been extensively studied (Yang et al., 2014). A close association exists between selenium and GPX4. Selenium protects GPX4 against irreversible inactivation (Friedmann Angeli and Conrad, 2018). When the selenium contained in GPX4 was replaced with sulfur in mice, survival was ≤ 3 weeks because of the development of neurological complications (Wirth et al., 2010). Furthermore, selenium increased GPX4 levels and protected cells from damage caused by oxidative stress, thereby inhibiting ferroptosis (Ingold et al., 2017).

Recent research has confirmed that intracerebroventricular injection of sodium selenite (SS) significantly improved neurological recovery in a mouse model of ICH (Alim et al., 2019). We hypothesized that SS would also effectively improve neurological recovery after SCI induction. In this study, we evaluated the neural protective effects of SS in a rat model of SCI, investigated the changes in factors essential for ferroptosis, and determined whether GPX4 and ferroptosis were targets by which SS exerted its effects on neural repair.

Materials and Methods

Experimental animals

The urethra of female rats is short and wide, which is convenient for micturition management after spinal cord injury. Therefore, this study was conducted with 10-week-old, female Wistar rats (220 ± 20 g). The rats were acquired from Sibeifu Biotechnology Co., Ltd. (Beijing, China; license No. SCXK [Jing] 2019-0010). The rats were maintained in a temperature- and humidity-controlled room with a 12-hour dark/light cycle and free access to water and food. The Institutional Animal Care and Use Committee of Capital Medical University (Beijing, China) approved this study (approval No. AEEI-2019-041) on March 25, 2019. The study was conducted in accordance with the Committee for the Purpose of Control and Supervision of Experimentation on Animals (CPCSEA) guidelines.

SS preparation

SS (Na_2O_3Se, product number S5261) was purchased from Sigma-Aldrich Trading Co., Ltd. (Shanghai, China). The SS powder was dissolved in normal saline at a stock concentration of 10 μM and diluted to working concentrations of 5 and 2.5 μM. The stock solutions of SS were frozen at –20°C. In accordance with the product description, the working aliquots were stored at 2–8°C for 30 days to maintain activity.

Experimental design

A preliminary experiment was conducted prior to the formal experiments. The rats were treated with three doses of SS (2.5, 5, and 10 μM) (n = 4/dose) 10 minutes after the SCI model was established. The control group comprised rats that were not subjected to SS treatment. Twenty-four hours after establishment of the SCI model, a segment of the spinal cord with the injured area at its center was collected for biochemical examination. The results showed that the expression of Gpx4 mRNA was highest and malondialdehyde (MDA) was lowest in the 2.5 μM treatment group, indicating that this SS concentration had the greatest effect on ferroptosis-related factors after SCI. Therefore, 2.5 μM SS was chosen for subsequent experiments.

For the formal study, Wistar rats were randomized into three groups (n = 35): (1) Sham group in which laminectomy and exposure of the dura were carried out without contusion injury or SS injection; (2) SCI group, which was subjected to a spinal cord contusion at the T10 vertebral level and spinal cord injection with normal saline (3 μL); and (3) SS group, which was subjected to T10 contusion injury and spinal cord injection with SS (3 μL, 2.5 μM). The rats were sacrificed on days 1, 3, and 7 and week 8 following SCI, and molecular and biochemical analyses of the spinal cord samples were performed. Samples that were collected on day 1 were also analyzed by transmission electron microscopy. At 8 weeks after establishment of the model, the spinal cords were fixed with 4% paraformaldehyde and subjected to pathological and immunohistochemical analysis (**Figure 1A**).

Contusion SCI model, SS injection, and tissue collection

The contusion injury method used in this study was performed as previously reported (Qin et al., 2018). Anesthetization of rats was achieved by inhalation of isoflurane (2.5–5%; Ruiward Life Technology Co., Ltd.; Shenzhen, China) after which the rats were placed on the operating table in a prone position. After locating the T10 spinous process, their backs were shaved followed by sterilization. A 4 cm longitudinal midline incision was made, and the paraspinal muscles were stripped to expose the spinous processes and lamina (T9–T11). A laminectomy was conducted at the T10 vertebral level to expose the spinal dura mater. The scope of resection included the T10 spinous process, lamina, and part of the pedicles. The dorsal and lateral sides of the spinal dura mater were exposed to ensure the thoroughness of the laminectomy. Sterile forceps were used to clamp the T9 and T11 spinous processes, and rats in the SCI and SS groups underwent spinal cord contusion at the T10 level using an Infinite Horizon Impactor (IH-0400 Impactor; Precision Systems and Instrumentation, LLC; Natick, MA, USA). Programmable force levels (250 kdynes) and a standard rat tip impactor size (2.5 mm diameter) were used, and errors > 3% with regard to spinal dura mater tears and force levels were rejected. Successfully established SCI rat models were confirmed by the presence of strong lower limb contractions and tail-spasm swings as previously described (Hu et al., 2015). Subsequently, the surgical field was irrigated with sterile saline twice to avoid infection and clear the exposed area. Ten minutes after the contusion, SS or normal saline (3 μL) was injected into the T10 vertebra at an angle of 90° using a microsyringe (Quintessential Stereotaxic Injector; Cat# 53311; Stoelting Co., Chicago, IL, USA). Beginning at the dorsal surface of the spinal dura, the injection depth was 2 mm, and the injection time was 3 minutes. Blood vessels were avoided during injection. After injection, the needle was left in place for five minutes to prevent leakage and then slowly withdrawn. The wound was sutured in layers.

All surgical manipulations were carried out under aseptic conditions using an operating microscope (DRE Medical; Louisville, KY, USA). After closure of the incision, the rats were kept warm in an incubator until they fully recovered. Then, the animals were housed alone in cages and allowed access to food and water ad libitum. Bladder expression was manually conducted twice a day until the micturition reflex returned, and penicillin (40,000 U; Huabei Pharmaceutical Co., Ltd., Shijiazhuang, China) was intramuscularly injected following the operations.

For molecular and biochemical analysis, 40 mg/kg sodium pentobarbital solution (Sigma-Aldrich, St. Louis, MO, USA) was injected intraperitoneally to anesthetize the rats followed by transcardial perfusion with phosphate-buffered solution (PBS). Then, a 1.5-cm long spinal cord segment, including the injury epicenter (center of congestion and swelling), was resected and frozen in liquid nitrogen as described previously (Qin et al., 2018). For pathological, immunofluorescence, and immunohistochemical analysis, rats were anesthetized with intraperitoneal pentobarbital sodium injection, transcardiac perfusion was performed with saline followed by 4% paraformaldehyde, and the spinal cord samples were resected and stored in 4% paraformaldehyde at 4°C.

Rats were sacrificed on days 1, 3, and 7 post-surgery, and spinal cord samples were harvested immediately and fresh frozen in liquid nitrogen followed by molecular and biochemical analysis. At 8 weeks after injury, rats were sacrificed and spinal cord samples were collected for preparation of paraffin sections. Then, 5-μm-thick sections were dewaxed with xylene and anhydrous alcohol and stained.

Basso, Beattie and Bresnahan locomotor rating scale scores

Functional recoveries of hind limbs were assessed by the Basso, Beattie, and Bresnahan (BBB) locomotor rating scale (Basso et al., 1995). The BBB scores ranged from 0 to 21, and each rat was positioned in an open field for 5 minutes and allowed to habituate by freely exploring prior to the assessment. The BBB scores were assessed immediately (time 0) and then once per week for 8 weeks post-surgery, and these assessments were conducted by two independent observers who were blinded to the experimental groups.

Gait analysis

Gait analysis was performed 1 day before contusion injury and at week 8 postoperatively (the endpoint of the experiment). Quantification of gait data was performed using the DigiGait Imaging System (Mouse Specifics, Boston, MA, USA). Briefly, DigiGait™ automatically identified and analyzed gaits from the underside of the rats as they walked on a treadmill and generated more than 50 metrics. In this study, the treadmill speed was 10 cm/second, and all dynamic gait indices were calculated using the DigiGait analysis software. The indices that were analyzed included paw area, hind limb shared stance time, stance duration, stride duration, stride frequency, stride length, and gait symmetry. The paw area refers to the maximal paw area that was in contact with the treadmill during the stance phase of the step cycle. The hind limb shared stance time refers to the time that both hind limbs were in contact with the belt. Stance duration refers to the time during which the paw remained in contact with the belt. Stride duration refers to the amount of time required for one limb to complete a single stride. Stride frequency refers to the number of complete stride cycles performed by one paw per second. Stride length refers to the distance between the initial contacts of the same paw in one complete stride cycle of the hind limbs. The formula by which gait symmetry was calculated is as follows: (right forelimb step frequency + left forelimb step frequency)/(right hind limb step frequency + left hind limb step frequency). A gait symmetry value closer to 1 represented improved coordination of forelimbs and hind limbs.

Transmission electron microscopy

Spinal cord tissue samples from the three groups were collected at 24 hours after injury, and the samples were immersed in a solution of 2% paraformaldehyde and 2% glutaraldehyde in 0.1 M sodium cacodylate, fixed in electron microscopy fixation liquid containing 1% osmium tetroxide/0.1 M phosphate buffer (pH 7.4), and dehydrated in alcohol and acetone. After embedding in epoxy resin, the samples were polymerized for 48 hours at 60°C. Ultrathin sections (60–80 nm) were cut using an ultramicrotome and stained with 2% uranium acetate saturated alcohol solution and lead citrate. Transmission electron microscopy (HT7700; Hitachi, Tokyo, Japan) was used for imaging.

Evaluation of iron levels

Iron concentrations in spinal cord specimens were determined on days 1, 3, and 7 after injury using an iron assay kit (A039-2; Nanjing Jiancheng Bioengineering Institute, Nanjing, China) following the manufacturer's instructions. Briefly, samples were homogenized and heated in a boiling water bath for 5 minutes to coagulate proteins. The cold homogenates were centrifuged for 10 minutes at 986 × *g*, the supernatants were collected, and the optical densities (OD) were measured at 520 nm using a spectrophotometer (752-P; Shanghai Xian Ke, Shanghai, China). The relative iron concentration was calculated using the protein level in the spinal cord specimen as a reference.

Determination of MDA concentrations

MDA levels in spinal cord specimens were evaluated on days 1, 3, and 7 post-injury using an MDA assay kit (A003-1, Nanjing Jiancheng Bioengineering Institute) following the manufacturer's instructions. Briefly, the samples were vortexed after which the tube mouth was sealed with preservative film, and a small hole was drilled with a needle. The tubes were placed in a boiling water bath for 40 minutes, cooled, and centrifuged for 10 minutes at 986–1127 × *g*. The ODs of the resulting supernatants were measured at 532 nm with a spectrophotometer (Leidu Life Technology Co., Ltd., Shenzhen, China).

Determination of glutathione concentrations

Glutathione (GSH) concentrations in the T10 spinal cord specimens were measured on days 1, 3, and 7 post-injury using a GSH assay kit (A006-2, Nanjing Jiancheng Bioengineering Institute). Briefly, supernatant (0.1 mL) from the spinal cord homogenate was added to 0.1 mL of reagent 1, and the samples were centrifuged for 10 minutes at 986 × *g*. After centrifugation, the supernatants were collected. Sample detection was performed in accordance with the kit instructions. After the color reaction, the absorbance values at 405 nm were measured using a microplate reader (BioTek Epoch, Winooski, VT, USA). The absorbance values for the blank, standard, and experimental wells were recorded, and the experiments were repeated three times. The GSH concentrations were calculated according to the following formula: GSH concentration = (measured OD value – blank OD value)/(standard OD value – blank OD value) × GSH standard concentration (20 μM) × dilution factor / protein concentration of homogenate.

Determination of GPX activity

GPX activity in spinal cord tissue was determined using a GPX activity assay kit (A005, Nanjing Jiancheng Bioengineering Institute) as instructed by the manufacturer. OD values for each group were measured at 412 nm, and GPX activities were calculated.

Western blot analysis

The T10 spinal cord samples were homogenized in radioimmunoprecipitation assay lysis buffer (Servicebio, Wuhan, China) supplemented with protease inhibitors using a tissue homogenizer (Servicebio). The protein levels were evaluated with a bicinchoninic acid kit (Servicebio). Following denaturation, equal protein amounts were separated using sodium dodecyl sulfate polyacrylamide gel electrophoresis (10% gels). After electrophoresis, the proteins were transferred to polyvinylidene fluoride membranes (Millipore, Billerica, MA, USA), which were blocked for 1 hour at room temperature using Tris-buffered saline-Tween 20 containing 5% skim milk. Primary antibodies were diluted, added to the membranes, and incubated at 4°C overnight. The primary antibodies used in this study are shown in **Table 1**. The membranes were washed with Tris-buffered saline-Tween 20 followed by incubation with a secondary antibody (horseradish peroxidase [HRP]-conjugated goat anti-mouse IgG; 1:5000; Servicebio, Cat# GB23301, RRID: AB_2904020 or HRP-conjugated goat anti-rabbit IgG; 1:5000; Servicebio, Cat# GB23303, RRID: AB_2811189) at room temperature for 30 minutes. After protein imaging with electrogenerated chemiluminescence reagents (Servicebio), the bands were scanned, and the ODs of the target bands were determined using AlphaEaseFC 4.0 imaging software (Alpha Innotech, San Leandro, CA, USA). For quantitative analysis, relative expression was normalized to the OD of β-actin bands.

Quantitative reverse transcriptase-polymerase chain reaction

Total RNA extraction from spinal cord tissues was performed using a total RNA extraction kit (Servicebio). RNA concentrations and purity were determined by NanoDrop 2000 spectrophotometry (Thermo Fisher Scientific, Wilmington, DE, USA), and the RNA extracts were diluted to equal concentrations. Ten μL of RNA were used for complementary DNA synthesis via the Servicebio® RT First-Strand cDNA Synthesis Kit. Standard quantitative reverse transcriptase-polymerase chain reaction (qRT-PCR) was conducted using the CFX96 Real-Time PCR Detection System (Bio-Rad, Hercules, CA, USA). Each reaction included 7.5 μL 2× SYBR Green qPCR Master Mix (no ROX), 1.5 μL forward and reverse primers, 2 μL complementary DNA, and 4 μL ddH_2O. The instrument settings were as follows: initial denaturation for 10 minutes at 95°C and 40 cycles of 95°C for 15 seconds and 60°C for 60 seconds. The mRNA levels were evaluated by the $2^{-\Delta\Delta CT}$ method (Livak and Schmittgen, 2001), and Gapdh served as the reference for normalization. Three replicates were analyzed for each sample per gene. **Table 2** shows the primer sequences that were used.

Table 1 | **Primary antibodies used in this study**

Antibody	Host	Dilution	Catalog No.	RRID	Supplier	Application
GPX4	Rabbit	1:2000	ab125066	AB_10973901	Abcam	WB
SP1	Mouse	1:1000	sc-420	AB_628271	Santa	WB, IF
4-HNE	Rabbit	1:3000	ab46545	AB_722490	Abcam	WB
NeuN	Mouse	1:200	GB13138-1	AB_2904014	Servicebio	IF
GFAP	Rabbit	1:800	GB11096	AB_2904015	Servicebio	IF
CNPase	Rabbit	1:50	13427-1-AP	AB_2082477	Proteintech	IHC
β-actin	Mouse	1:1000	GB12001	AB_2904016	Servicebio	WB

4-HNE: 4-Hydroxynonenal; CNPase: 2', 3'-cyclic adenylate-3'-phosphodiesterase; GAPDH: glyceraldehyde-3-phosphate dehydrogenase; GFAP: glial fibrillary acidic protein; GPX4: glutathione peroxidase 4; IF: immunofluorescence; IHC: immunohistochemistry; NeuN: neuronal nuclear antigen; SP1: specificity protein 1; WB: western blot assay.

Table 2 | **Primers for real-time quantitative polymerase chain reaction**

Gene	Primer sequence (5'–3')	Accession number	Product size (bp)
ACSL4	Forward: TCA AGC ATT CCT CCA AGT AGA CC	NM_053623.1	236
	Reverse: CAG CCG TAG GTA AAG CAG GAG		
LPCAT3	Forward: CCT ACT TCT ATG GAG CCT TCT TGG T	NM_001012189.1	224
	Reverse: AGG GCG GGT ATC ATA GTC TTC A		
GPX4	Forward: GCC GAG TGT GGT TTA CGA ATC	NM_001039849.3	257
	Reverse: ACG CAG CCG TTC TTA TCA ATG		
SP1	Forward: CCA GAC CAT TAA CCT CAG TGC A	NM_012655.2	142
	Reverse: ATG TAT TCC ATC ACC GCC AG		
GAPDH	Forward: CTG GAG AAA CCT GCC AAG TAT G	NM_017008.4	138
	Reverse: GGT GGA AGA ATG GGA GTT GCT		

ACSL4: Acyl-coenzyme A synthetase long-chain family member 4; GAPDH: glyceraldehyde-3-phosphate dehydrogenase; GPX4: glutathione peroxidase 4; LPCAT3: lysophosphatidylcholine acyltransferase 3; SP1: specificity protein 1.

Immunofluorescent staining

Antigen retrieval within spinal cord sections was conducted using a citric acid buffer solution (pH 6). The sections were circled using a marking pen, and autofluorescence quencher solutions (G1221, Servicebio), which effectively reduce spontaneous tissue fluorescence and improve the signal-to-noise ratio of immunofluorescence detection, were added to the circles followed by 5 minutes of incubation. After washing for 10 minutes, the sections were incubated with bovine serum albumin (Servicebio) for 30 minutes. Diluted primary antibodies (**Table 1**) were added dropwise, and the sections were incubated overnight at 4°C. After washing with PBS, the sections were incubated with the corresponding secondary antibodies (Alexa Fluor® 488-conjugated goat anti-mouse IgG; 1:400; Servicebio, Cat# GB25301, RRID: AB_2904018 or Cy3-conjugated goat anti-rabbit IgG; 1:300; Servicebio, Cat# GB21303, RRID: AB_2861435) for 50 minutes in the dark at room temperature. After three washes with PBS, the nuclei were stained with 4′,6-diamidino-2-phenylindole for 10 minutes. Then, the sections were sealed with an anti-fluorescence quenching medium. The numbers of neuronal nuclear antigen (NeuN)-positive cells and glial fibrillary acidic protein (GFAP)-positive cells were imaged by fluorescence microscopy (Eclipse C1; Nikon, Tokyo, Japan).

Immunohistochemistry

Antigen retrieval within spinal cord sections was conducted using ethylenediaminetetraacetic acid buffer (pH 9.0). The sections were incubated with 3% hydrogen peroxide at room temperature for 25 minutes in the dark to block endogenous peroxidase activity. Then, bovine serum albumin was added followed by a 30 minute incubation. Diluted primary antibodies (**Table 1**) were added dropwise, and the sections were incubated at 4°C overnight. The sections were washed with PBS, the corresponding secondary antibodies (described above) were added to the encircled sections, and the sections were incubated for 50 minutes in the dark at room temperature. Color development was performed with 3,3′-diaminobenzidine, and the nuclei were stained with hematoxylin for 3 minutes. After dehydration, the sections were mounted with neutral gum and imaged by microscopy (XSP-C204; Chongqing Scope Instrument Co., Chongqing, China). After hematoxylin staining, nuclei appeared blue, while positive expression of 3,3′-diaminobenzidine appeared brownish yellow. The number of 2′,3′-cyclic nucleotide 3′ phosphodiesterase (CNP)-positive cells in the SCI group was calculated.

Histological analysis

The spinal cord samples were embedded in paraffin and cut into 5-μm-thick sections. The sections were stained with hematoxylin-eosin reagents (Servicebio). The results were observed using an optical microscope (Eclipse E100; Nikon) and included the number of cells, arrangement regularity, and cavity sizes.

Statistical analysis

GraphPad Prism 7.0 (GraphPad Software, Inc., San Diego, CA, USA; www.graphpad.com) and SPSS (IBM SPSS Statistics for Windows (2015), version 23.0; IBM Corp., Armonk, NY, USA) software programs were used for analyses. Between-group comparisons were performed using the nonparametric Scheirer-Ray-Hare test with Dunn's *post hoc* test. Data are shown as median and interquartile range, and $P < 0.05$ denoted significance.

Results

SS improves hind limb locomotion recovery in rats with SCI

Figure 1B shows the BBB scores of rats in the three groups as a function of time post-SCI. Immediately following SCI, rats in the SCI and SS groups exhibited severe hind limb paralysis. Hind limb motor function began to recover at 1 week after SCI and showed a gradual increase during the 8-week experimental period. The BBB scores of the SS group were higher relative to those of the SCI group at each assessment point from 2–8 weeks after SCI. These results suggested that SS treatment promoted functional recovery after SCI.

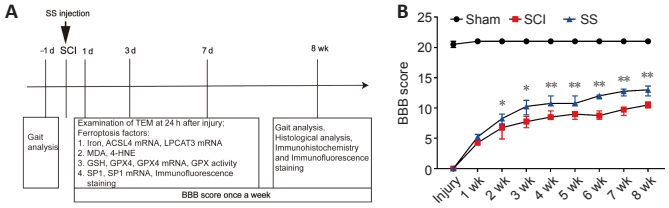

Figure 1 | **SS treatment improves recovery of hind limb motor function in SCI rats.**
(A) Design of the study. The baseline gait analysis data were obtained 1 day before the experiment. The rats were allocated into three groups (Sham, SCI, and SS groups). In the SS group, 3 μL of SS (2.5 μM) was injected into the spinal cord 10 minutes after SCI. Transmission electron microscopy was used to assess the injured spinal cord 24 hours after contusion. Western blot analysis, real-time quantitative polymerase chain reaction, immunofluorescent staining, and other methods were used to detect changes in factors related to ferroptosis on days 1, 3, and 7 after SCI. Hematoxylin-eosin, immunofluorescent, and immunohistochemistry staining were performed 8 weeks after injury. The BBB scores were evaluated each week until the 8th week, and gait analysis was performed again at the 8th week. (B) Alterations in BBB scores for rat hind limbs. The BBB scores for hind limbs in the SS group were significantly higher than those in the SCI group beginning at week 2 after injury. The data are shown as medians and interquartile ranges ($n = 6$). *$P < 0.05$, **$P < 0.01$, *vs.* SCI group (Scheirer-Ray-Hare test followed by Dunn's *post hoc* test). 4-HNE: 4-Hydroxynonenal; ACSL4: acyl-coenzyme A synthetase long-chain family member 4; BBB: Basso, Beattie and Bresnahan locomotor rating scale; GPX4: glutathione peroxidase 4; GSH: glutathione; LPCAT3: lysophosphatidylcholine acyltransferase 3; MDA: malondialdehyde; SCI: spinal cord injury; SP1: specificity protein 1; SS: sodium selenite; TEM: transmission electron microscope.

Baseline gait imaging was performed 1 day before SCI and repeated 8 weeks after SCI at a predetermined speed of 10 cm/s. Typical gait images of rats from the three groups at 8 weeks post-SCI are shown in **Figure 2A**. At 8 weeks after establishment of the model, the SCI group demonstrated a significant decrease in hind limb paw area ($P = 0.004$), and SS treatment ameliorated this loss ($P = 0.006$; **Figure 2B**). Gait analysis revealed a marked decrease in hind limb shared stance time in the SCI and SS groups ($P = 0.004$, $P = 0.037$) relative to that in the Sham group. In addition, the hind limb shared stance time in the SS group was significantly greater than that in the SCI group ($P = 0.004$; **Figure 2C**). The hind limb stance duration and stride duration of the rats in the SCI group were markedly lower than those in the Sham group ($P = 0.008$, $P = 0.01$), and SS treatment did not result in significant improvements ($P = 0.109$, $P = 0.078$; **Figure 2D** and **E**). A distinct increase in hind limb stride frequency in the SCI group ($P = 0.013$) was observed relative to that in the Sham group at 8 weeks post-injury; however, SS treatment did not alleviate this change ($P = 0.055$; **Figure 2F**). Stride length was significantly reduced in the SCI at 8 weeks after injury ($P = 0.01$), but the effect of SS treatment did not reach statistical significance ($P = 0.092$, **Figure 2G**). Compared with that in the Sham group, SCI significantly increased gait symmetry after 8 weeks ($P = 0.006$), and SS administration significantly alleviated this alteration ($P = 0.02$; **Figure 2H**).

SS improves hemolysis and ferroptosis-specific microstructural changes in spinal cord tissue after SCI

We evaluated the tissue ultrastructure in transverse sections of spinal cords 24 hours post-injury by transmission electron microscopy (**Figure 3**). In the SCI group, hemolysis was visible in the spinal cord tissue, and typical manifestations of ferroptosis were observed, including shrunken mitochondria, increased membrane density, and occasionally disrupted outer membranes. Hemolysis and characteristic manifestations of ferroptosis in the SS group were markedly decreased when compared with that in the SCI group, whereas none of these features were identified in the Sham group. Neither the SS group nor the SCI group exhibited typical manifestations of apoptosis, such as apoptotic bodies.

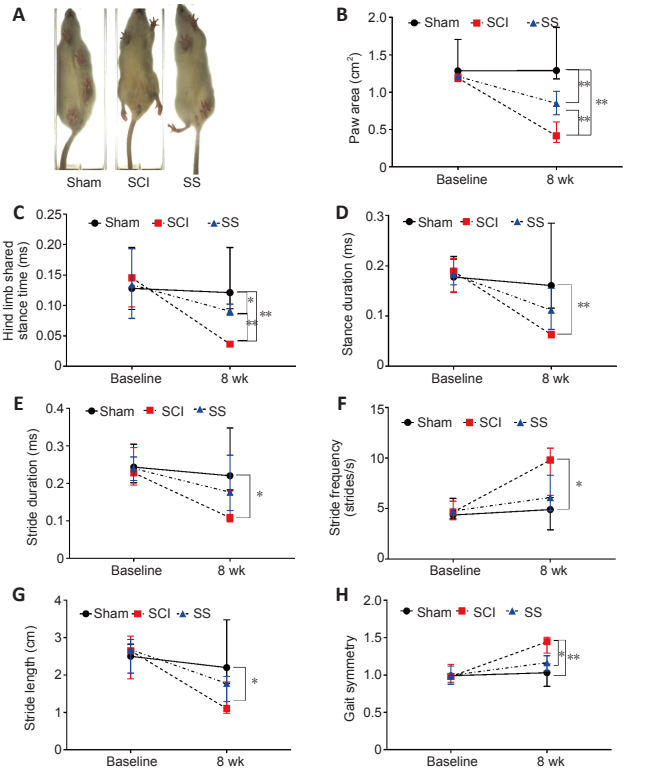

Figure 2 | **Effects of SS on gait analysis indices in rats 8 weeks after SCI.**
(A) Representative gait images for the three groups of rats. Changes in (B) paw area, (C) hind limb shared stance time, (D) stance duration, (E) stride duration, (F) stride frequency, (G) stride length, and (H) gait symmetry. The data are presented as medians and interquartile ranges ($n = 6$). *$P < 0.05$, **$P < 0.01$ (Scheirer-Ray-Hare test followed by Dunn's *post hoc* test). SCI: Spinal cord injury; SS: sodium selenite.

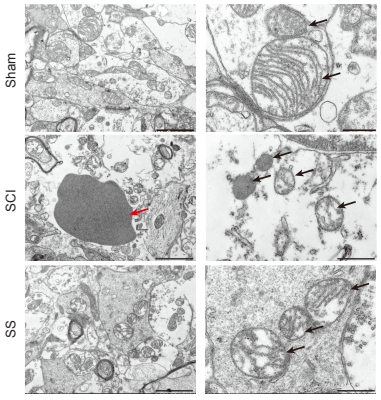

Figure 3 | **Effect of SS on hemolysis and ferroptosis-specific mitochondrial changes after spinal cord injury.**
Representative transmission electron microscopy images show spinal cord tissues from the SCI and Sham groups 24 hours after injury. Hemolysis, mitochondrial shrinkage, and other typical ferroptosis-related manifestations were observed in the SCI group. The red arrow indicates hemolysis, and the black arrows indicate mitochondria. Scale bars: left, 2 μm; right, 500 nm. SCI: Spinal cord injury; SS: sodium selenite.

SS treatment affects factors essential for ferroptosis in spinal cord tissues after SCI

Iron concentrations, *Acsl4* and *Lpcat3* mRNA expression, MDA levels, and HNE expression were detected at 1, 3, and 7 days after SCI. Relative to that in the Sham group, the SCI group showed markedly higher iron levels ($P < 0.05$), and iron concentrations in the SS group were statistically lower than that in the SCI group at 7 days after injury ($P = 0.037$; **Figure 4A**). These data indicated that iron overload may have been a critical factor that triggered ferroptosis after SCI, which was alleviated by SS treatment.

ACSL4 and LPCAT3 are involved in the biosynthetic pathway of PUFAs and can induce ferroptosis *in vivo* (Doll et al., 2017; Kagan et al., 2017). RT-qPCR demonstrated that *Acsl4* and *Lpcat3* mRNA expression was upregulated in spinal cord tissues of the SCI group compared with expression in the Sham group on days 1 and 3 post-injury ($P < 0.05$); however, differences between the two groups 7 days after injury were insignificant ($P > 0.05$). Moreover, SS treatment did not significantly affect *Acsl4* and *Lpcat3* mRNA expression ($P > 0.05$; **Figure 4B** and **C**). Considering that ACSL4 and LPCAT3 are associated with lipid peroxidation (Doll et al., 2017; Kagan et al., 2017), we examined the lipid peroxidation products MDA and 4-hydroxynonenal (4-HNE) in the three groups after SCI. MDA and 4-HNE levels were markedly elevated in spinal cord tissues from the SCI group compared with those from the Sham group ($P < 0.05$), and SS treatment partially alleviated this change ($P < 0.05$; **Figure 4D–F**). Taken together, the above results demonstrated that lipid peroxidation catalyzed by ACSL4 and LPCAT3 occurred in spinal cord tissues after SCI, and SS treatment decreased the iron concentration and levels of

lipid peroxidation. However, ACSL4, and LPCAT3 do not appear to be targets of SS.

As a crucial molecule in the signaling pathway that regulates ferroptosis, GPX4 catalyzes the reduction of lipid peroxides. GPX4 inactivation is one of the key features of ferroptosis, and this inactivation occurs either by decreasing GSH levels or by directly targeting GPX4 (Dixon and Stockwell, 2019). Relative to that in the Sham group, the SCI group exhibited significantly lower GSH expression at all time points post-injury ($P < 0.05$), and GPX4 expression was significantly decreased on days 1 and 3 after injury ($P < 0.05$). Additionally, SS treatment led to statistically significant improvement in GSH and GPX4 expression ($P < 0.05$; **Figure 4G–I**).

Together, major factors in the ferroptosis pathway, including iron, ACSL4, LPCAT3, MDA, 4-HNE, and the GSH/GPX4 axis, were linked to secondary injury associated with SCI. Furthermore, SS treatment suppressed ferroptosis by inhibiting iron accumulation, activating GPX4, and curbing lipid peroxidation.

Possible mechanisms by which SS improves neural function recoveries after SCI

We determined the biomechanism by which SS promoted GPX4 expression and inhibited ferroptosis. *Sp1* and *Gpx4* mRNA and protein expression and GPX enzymatic activity was analyzed on days 1, 3, and 7 after SCI. Relative to expression in the Sham group, the SCI group showed markedly lower GPX4 protein and *Gpx4* mRNA expression (**Figures 4H**, **I** and **5A**). GPX activity was also reduced by injury (**Figure 5B**). SS treatment led to marked increases in these indicators.

Western blot, RT-qPCR, and immunofluorescent staining revealed that SP1 protein and mRNA expression was decreased after SCI, most noticeably within 3 days, and SS treatment improved the expression of these molecules substantially at all three time points post-injury (**Figure 5C–G**). Taken together, SS may upregulate GPX4 expression by increasing the expression of the transcription factor SP1, thereby enhancing GPX4 activity, suppressing ferroptosis, and promoting neurological recovery after SCI.

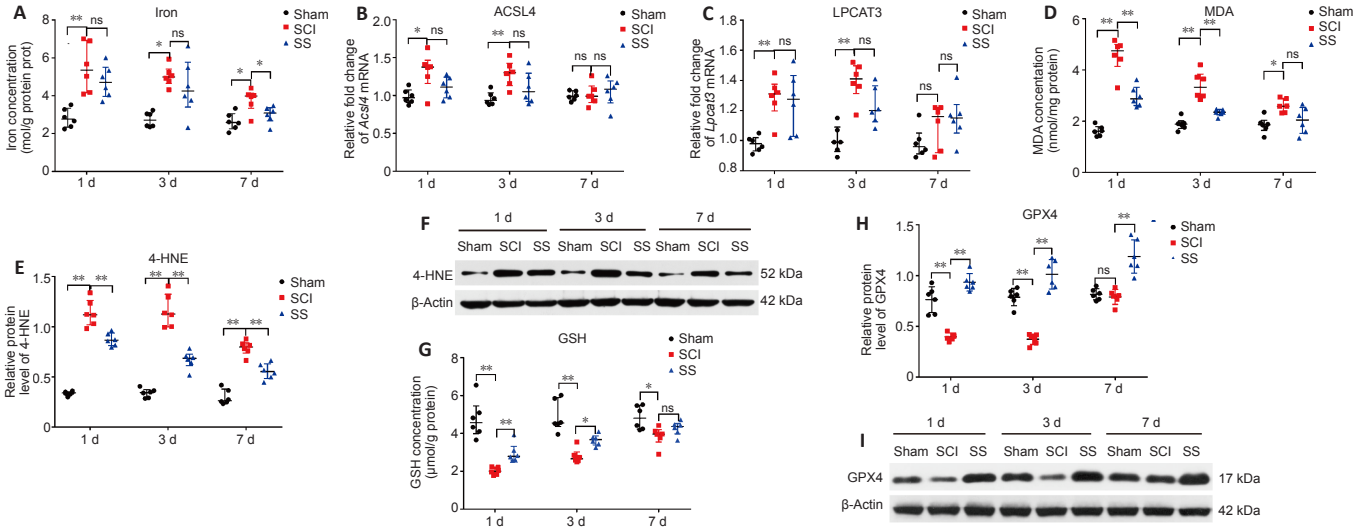

Figure 4 | **SS-mediated changes in factors essential for ferroptosis in spinal cord tissues after SCI.**
(A) The iron concentrations in the SCI group were markedly elevated compared with that in the Sham group, while SS treatment alleviated this change on day 7 after injury. (B, C) RT-qPCR demonstrated that *Acsl4* and *Lpcat3* mRNA expression was upregulated in spinal cord tissues after injury, while SS administration had no obvious effect on these changes. (D) MDA levels were increased following injury, and SS alleviated this elevation at the injury site. (E, F) The 4-HNE levels were increased after SCI. Relative to that in the SCI group, 4-HNE levels in the SS group were markedly decreased. (G) GSH levels were significantly decreased after injury compared with that in the Sham group, and SS treatment led to significant improvement. (H, I) GPX4 levels decreased after SCI compared with levels in the Sham group but increased significantly after SS treatment. Western blot band intensities were normalized to those of β-actin. The data are shown as medians and interquartile ranges ($n = 6$). $^*P < 0.05$, $^{**}P < 0.01$ (Scheirer-Ray-Hare test followed by Dunn's *post hoc* test). 4-HNE: 4-Hydroxynonenal; ACSL4: acyl-coenzyme A synthetase long-chain family member 4; GPX4: glutathione peroxidase 4; GSH: glutathione; LPCAT3: lysophosphatidylcholine acyltransferase 3; MDA: malondialdehyde; ns: not significant; qRT-PCR: quantitative reverse transcriptase-polymerase chain reaction; SCI: spinal cord injury; SS: sodium selenite.

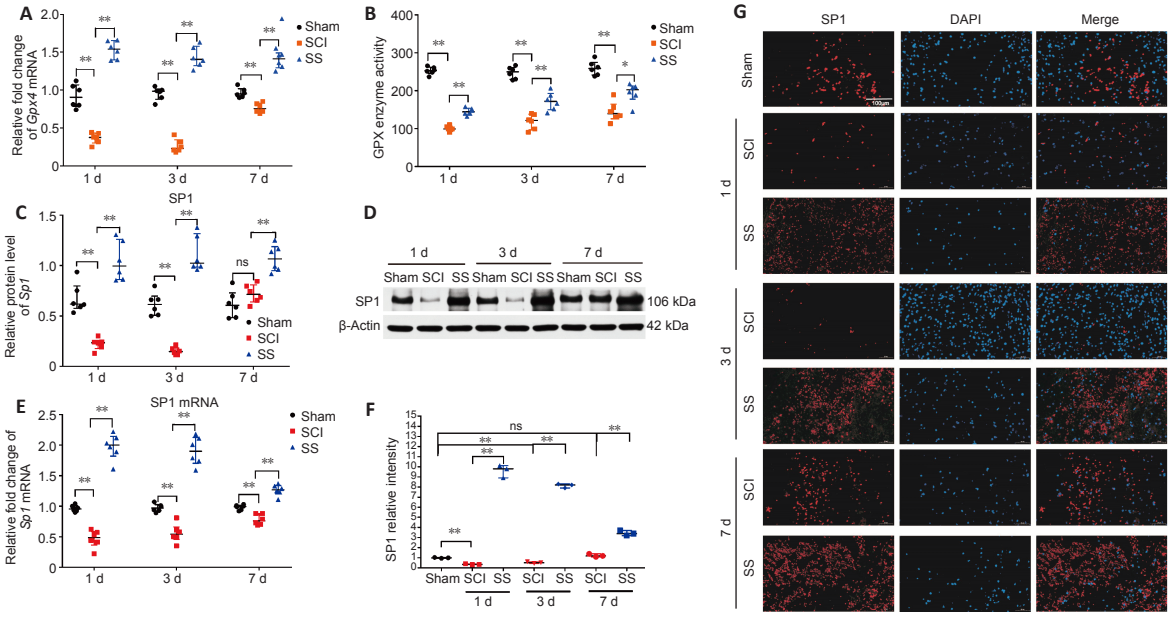

Figure 5 | **Possible mechanisms by which SS improve GPX4 expression after SCI.**
(A) RT-qPCR showed that the *Gpx4* mRNA level significantly decreased after SCI but markedly increased after SS treatment. (B) GPX enzymatic activity showed a pattern similar to *Gpx4* mRNA expression. (C, D) SP1 protein levels decreased on days 1 and 3 following SCI but significantly increased after SS treatment at each observation time point. Western blot band intensities were normalized to those of β-actin. (E) *Sp1* mRNA expression showed patterns similar to that observed by western blot for SP1 protein expression in each group. The effects of SS on SP1 immunofluorescence at 1, 3, and 7 days after SCI were explored. Immunofluorescent images of transverse sections were captured at the center of the injured spinal cord. (F) Quantification of SP1 expression in the epicenter of injury. The data are shown as medians and interquartile ranges ($n = 6$). $^{**}P < 0.01$ (Scheirer-Ray-Hare test followed by Dunn's *post hoc* test). (G) Representative fluorescent micrographs of SP1 staining (red, Cy3) and nuclei (blue, DAPI) in the epicenter of the injured spinal cord. SP1 expression in the SCI group was decreased compared with that in the Sham group, whereas the expression of SP1 in the SS-treated group was dramatically higher than that in the SCI group. Scale bar: 100 μm. DAPI: 4′,6-Diamidino-2-phenylindole; GPX4: glutathione peroxidase 4; ns: not significant; SCI: spinal cord injury; SP1: specificity protein 1; SS: sodium selenite.

SS promotes spinal cord repair after SCI

Hematoxylin-eosin staining of spinal cord tissues at 8 weeks post-injury is shown in **Figure 6**. The structures of spinal cord tissues in the Sham group were basically normal, whereas the SCI group displayed spinal cord tissue breakdown, scar connections, structural disorder, and obvious cavity formation. Comparatively, the cavities within the spinal cord tissues of the SS group were significantly reduced, and tissue arrangement demonstrated greater regularity. Thus, we inferred that SS promoted repair of injured spinal cord tissue and, subsequently, improved hind limb motor function.

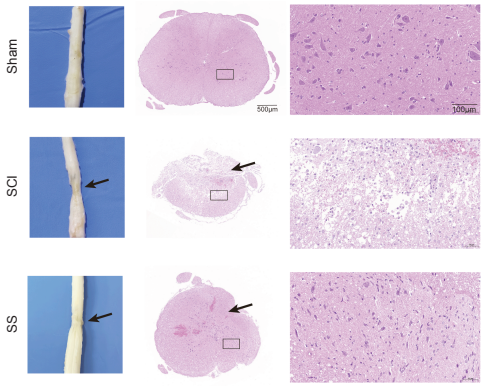

Figure 6 | **Effects of SS treatment on spinal tissue repair after SCI.**
Hematoxylin-eosin staining was performed on cross sections of the injury epicenter 8 weeks after SCI. The nuclei are blue, and the cytoplasm is red. Representative images showed obvious cavities and tissue disorder (arrows) in the SCI group. In contrast to the SCI group, the cavities were significantly reduced, and the tissue arrangement was more regular in the SS group. Scale bars: 500 μm (middle panels), 100 μm (right panels). SCI: Spinal cord injury; SS: sodium selenite.

SS increases the number of NeuN$^+$ and CNP$^+$ cells but decreases the number of GFAP$^+$ cells after SCI

We performed immunofluorescent staining and immunohistochemical analysis to identify potential target cells that may benefit from SS treatment in rats with SCI. Immunofluorescent staining revealed that the numbers of NeuN$^+$ cells in the SCI group were significantly decreased relative to that in the Sham group at 8 weeks post-injury, whereas the numbers of NeuN$^+$ cells in the SS group were increased compared with that in the SCI group. In comparison, the numbers of GFAP$^+$ cells in the SCI group were substantially higher relative to those in the Sham group at 8 weeks after injury, whereas the SS group showed a slight increase (**Figure 7A–C**). The differences between the SCI and SS groups were statistically significant for both proteins.

Immunohistochemical results demonstrated that the numbers of CNP$^+$ cells in the SCI group were markedly decreased compared with those in the Sham group at 8 weeks after injury (**Figure 7D**). SS treatment caused a substantial increase in the numbers of CNP$^+$ cells compared with that in the SCI group. Because CNP is a specific marker of oligodendrocytes and myelinated fibers (Müller and Seifert, 1982), we concluded that SS treatment protected oligodendrocytes during the pathology of SCI.

Discussion

Cell death is a major contributor to secondary injury associated with SCI, and the mechanisms of cell death include apoptosis, necrosis, and ferroptosis (Shi et al., 2021). Inhibition of ferroptosis represents a theoretically feasible treatment for SCI. Previous studies on iron chelators and specific lipid peroxidation scavengers have demonstrated that ferroptosis inhibitor significantly improved the motor function of SCI rats (Yao et al., 2019; Zhou et al., 2020). Our results indicated that ferroptosis occurred in spinal cord lesions after contusion. Furthermore, several factors that initiate and regulate ferroptosis exhibited SCI-induced alterations, while SS intervention effectively ameliorated these changes. The histomorphological and staining results observed in this study also support similar conclusions. The present study showed that SS exerted neuroprotective effects after SCI. More importantly, for the first time, we demonstrated that the neuroprotective effects of SS may be achieved by inhibiting ferroptosis mediated by GPX4.

Data from BBB scores and gait analysis showed that SS administration after SCI enhanced hind limb locomotion recovery, which agrees with results from previous studies (Yeo et al., 2008; Chen et al., 2013). However, it should be noted that this study focused on improvement of neurological function from the perspective of inhibiting ferroptosis rather than apoptosis. Using electron microscopic analysis, we observed that SCI caused numerous typical manifestations of ferroptosis, while SS intervention reduced these changes. Neither the SS group nor the SCI group exhibited typical manifestations of apoptosis. A previous study demonstrated that cell apoptosis occurred 1–2 days after injury (Nottingham and Springer, 2003), which may explain these results. SS administration significantly reduced empty cavities and resulted in more uniform tissue structure. In addition, SS administration increased the percentage of NeuN$^+$ and CNP$^+$ cells but decreased the number of GFAP$^+$ cells in spinal cord tissues. Thus, we suggest that SS promoted repair after

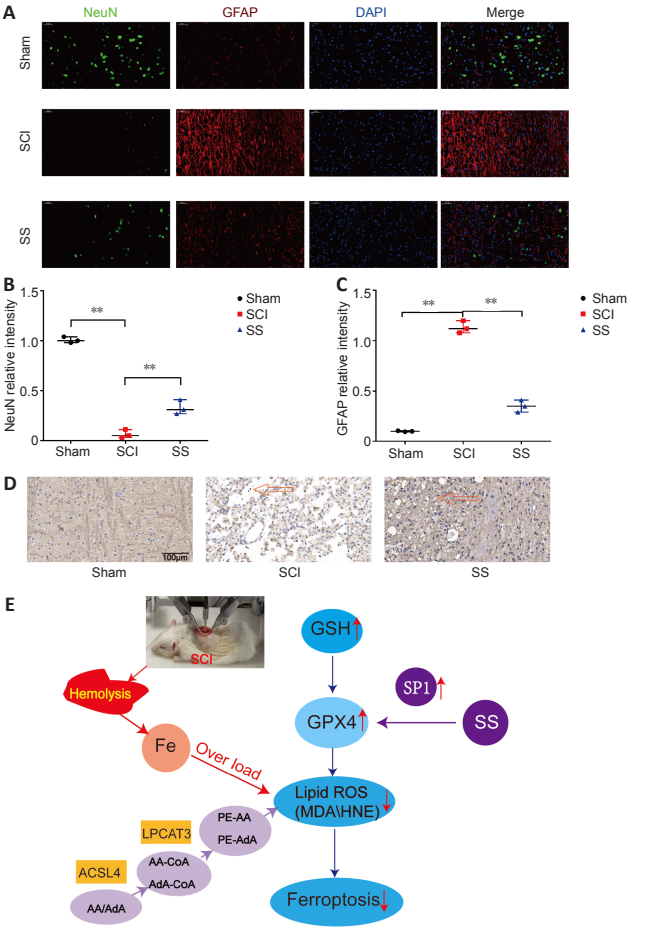

Figure 7 | **Effects of SS on the numbers of NeuN$^+$, GFAP$^+$, and CNP$^+$ cells after SCI.**
(A) The effect of SS on NeuN and GFAP immunofluorescence at 8 weeks after injury. Immunofluorescent images of NeuN$^+$ and GFAP$^+$ cells in the epicenter of injury were captured by fluorescence microscopy. Representative fluorescence micrographs of NeuN (green, Alexa Fluor 488), GFAP (red, Cy3), and nuclei (blue, DAPI) at the epicenter of injury. NeuN$^+$ cells in the SCI group were decreased compared with that in the Sham group, whereas NeuN$^+$ cells in the SS-treated group were increased relative to that in the SCI group. GFAP$^+$ cells in the SCI group were increased compared with that in the Sham group, whereas the GFAP$^+$ cells in the SS-treated group were decreased compared with that in the SCI group. Scale bar: 100 μm. (B, C) Quantification of NeuN$^+$ and GFAP$^+$ cells. The data are shown as medians and interquartile ranges (n = 3). $^{**}P < 0.01$ (Scheirer-Ray-Hare test followed by Dunn's *post hoc* test). (D) The effect of SS on CNP immunohistochemical staining at 8 weeks after injury. Images of the transected sections of the epicenter of injury were captured by microscopy. Representative micrographs of CNP staining (yellowish-brown) and nuclear staining (blue) at the epicenter of injury. CNP$^+$ cells in the SCI group were markedly decreased compared with that in the Sham group at 8 weeks after injury, whereas SS treatment caused a marked increase in the number of CNP$^+$ cells (arrows). Scale bar: 100 μm. (E) The possible mechanism by which SS promotes the recovery of neurological function in rats with SCI through GPX4. 4-HNE: 4-Hydroxynonenal; AA: arachidonic acid; AA-CoA: arachidonic acid-coenzyme A; ACSL4: acyl-coenzyme A synthetase long-chain family member 4; AdA: adrenic acid; AdA-CoA: adrenic acid-coenzyme A; CNPase: 2′,3′-cyclic nucleotide-3′-phosphodiesterase; DAPI: 4′,6-diamidino-2-phenylindole; GFAP: glial fibrillary acidic protein; GPX4: glutathione peroxidase 4; GSH: glutathione; LPCAT3: lysophosphatidylcholine acyltransferase 3; MDA: malondialdehyde; NeuN: neuronal nuclear antigen; PE-AA: phosphatidylethanolamine-arachidonic acid; PE-AdA: phosphatidylethanolamine- adrenic acid; ROS: reactive oxygen species; SCI: spinal cord injury; SP1: specificity protein 1; SS: sodium selenite.

SCI by preserving neurons and oligodendrocytes, which increased nerve fiber regeneration and remyelination, and by inhibiting reactive astrogliosis and glial scar formation.

To further investigate the mechanism by which SS protects neurons in rats with SCI, we conducted a study at the molecular level. The results revealed that the iron concentrations in injured spinal cord tissues were markedly elevated in the SCI group, and SS administration partially alleviated this increase. Iron chelators have previously been shown to inhibit ferroptosis by dramatically decreasing the iron load within spinal cord lesions (Yao et al., 2019). Therefore, the mechanistic action of SS may differ from that of iron chelators.

ACSL4 and LPCAT3 are key enzymes responsible for the synthesis and reconstruction of PUFAs that are incorporated into cell membrane phospholipids. Overexpression of these enzymes can increase the levels of substrates available for lipid peroxidation, which subsequently triggers ferroptosis (Doll et al., 2017; Kagan et al., 2017). RT-qPCR studies revealed

elevated expression of Acsl4 and Lpcat3 in spinal cord tissues after SCI, while SS administration had no effect on this change. Furthermore, MDA and 4-HNE levels were increased following SCI, but SS administration inhibited this increase at the injury site. In summary, we hypothesize that the target affected by SS during ferroptosis is located downstream of ACSL4 and LPCAT3 and is closely related to the elimination of lipid peroxidation.

Ferroptosis has become an important research topic in recent years, and the molecular mechanism of this process has been continuously studied. Among various ferroptosis regulatory molecules, GPX4 is considered to be the core regulator of ferroptosis. In contrast, the inactivation or inhibition of GPX4 leads to a breakdown in oxidation balance, and lipid peroxides are able to destroy the cell membrane structure and trigger ferroptosis (Dixon and Stockwell, 2019). To elucidate the relationship between SS treatment and GPX4, we investigated the changes in GPX4 levels after SCI and SS treatment. Following SCI, levels of components in the GPX4 pathway decreased sharply, which agrees with previous literature (Yao et al., 2019). Additionally, SS increased GPX4 expression and activity and ultimately improved neurological functions by suppressing ferroptosis.

Several signaling pathways regulate ferroptosis through GPX4, including the glutamate cystine reverse transporter system (system XC−)/GSH/GPX4 axis. System XC− is a heterodimer composed of the light chain subunit SLC7A11 (XCT) and heavy chain subunit SLC3A2 linked through disulfide bonds and mediates the 1:1 exchange of intracellular glutamate and extracellular cystine (Ji et al., 2018). Cystine is rapidly converted into L-cysteine inside cells, which is the raw material for the synthesis of GSH. Erastin inhibits system XC− resulting in the inhibition of GSH synthesis (Sato et al., 2018). The lack of GSH and GPX4 suppresses the removal of lipid peroxides, which then results in membrane damage and ferroptosis induction (Seiler et al., 2008; Hassannia et al., 2019).

In the ICH model, Alim et al. (2019) found that human brain cells autonomously regulated cell damage caused by hemorrhage through Se intake. Further studies showed that selenium upregulated the expression of GPX4, inhibited ferroptosis, and protected neurons through activation of the transcription cofactor SP1. The 3′ untranslated region of *GPX4* mRNA contains a selenocysteine insertion sequence element (Touat-Hamici et al., 2014). During translation, the UGA codon is usually read as the termination codon, while in the presence of the selenocysteine insertion sequence, the UGA codon encodes an active site selenocysteine (U46). This particular form of translation requires a unique protein system to guide the insertion of selenocysteine into GPX4 and other selenoproteins. Therefore, the expression of GPX4 is regulated by the availability of selenium (Min et al., 2018). Both SCI and ICH are central nervous system injuries; therefore, we speculated that selenium functioned via a similar mechanism in SCI. Our results suggest that SS may increase the levels of the transcription factor SP1 and upregulate the expression of GPX4, thus inhibiting ferroptosis (**Figure 7E**).

Selenium has been previously used in the treatment of SCI; however, its role in protecting neural function has been studied from the perspective of inhibiting ROS mediated apoptosis (Yeo et al., 2008) and upregulating the expression of cardiovascular neurological factor and its receptor (Chen et al., 2015). In this study, the role of selenium in improving neural function after SCI was analyzed for the first time from the perspective of inhibiting ferroptosis. It should be noted that selenium-mediated regulation of GPX4 and protection of neurons are complex multifactorial processes rather than single linear mechanisms. Therefore, the cross effects of various mechanisms, including different types of cell death, cell regeneration, microenvironmental changes, and oxidative stress regulation, may have influenced our experimental results.

Because of the short experimental time, there were limitations in the present study. For the selenium/SP1/GPX4 axis, we only demonstrated a positive correlation in their expression levels without determining direct binding relationships and exact mechanisms. Thus, the conclusions require verification by additional experiments, such as SP1 knockout or inhibitor studies. For ACSL4 and LPCAT3, we only measured mRNA expression without protein expression and activity levels of them. Because transcription, translation, and activity are not always linked, the conclusion that "ACSl4 and lpcat3 do not seem to be the targets of SS" is not reliable enough. Thus, experiments evaluating protein expression and activity levels of ACSL4 and LPCAT3 should be performed in future researches. In terms of gait analysis, more gait indices and time points should be considered to obtain greater detail and more reliable results. Only rat experiments were conducted in the present study to demonstrate the effectiveness of selenium. Subsequent studies should combine *in vivo* and *in vitro* experiments that include different types of SCI models. The sample size for each group was limited, and follow-up studies should include expanded sample sizes to provide more power to the results.

In the present study, SS was administered by local spinal cord injection, which may increase the risk of infection. Moreover, SS is reported to have a narrow safe concentration range for spinal cord injection, which may increase the likelihood of toxicity issues. Therefore, future studies will be required to explore safer and more effective methods for the administration of SS.

In summary, SCI increased the concentration of iron and lipid peroxidation levels and decreased the expression of GPX4, thus triggering the onset of ferroptosis. SS administration after SCI may increase the expression and activity of GPX4 by activating the transcription factor SP1, thereby suppressing ferroptosis and promoting neurological recovery.

Acknowledgments: *We thank all the members of the Department of Spinal and Neural Function Reconstruction, China Rehabilitation Research Center for the technical supports they offered.*

Author contributions: *Study design and concept: YXC, JJL, BL and YY; experiment implementation: YXC, TZ, SG and BL; provision of critical reagents and scientific input: JJL, DGY, LJD and FG; rat management: YXC, SG, BL, and MLY; data analysis and paper preparation: YXC and JJL. All authors approved the final version of the manuscript.*

Conflicts of interest: *The authors declare that they have no competing interests.*

References

Alim I, Caulfield JT, Chen Y, Swarup V, Geschwind DH, Ivanova E, Seravalli J, Ai Y, Sansing LH, Ste Marie EJ, Hondal RJ, Mukherjee S, Cave JW, Sagdullaev BT, Karuppagounder SS, Ratan RR (2019) Selenium drives a transcriptional adaptive program to block ferroptosis and treat stroke. Cell 177:1262-1279.e25.

Basso DM, Beattie MS, Bresnahan JC (1995) A sensitive and reliable locomotor rating scale for open field testing in rats. J Neurotrauma 12:1-21.

Bersuker K, Hendricks JM, Li Z, Magtanong L, Ford B, Tang PH, Roberts MA, Tong B, Maimone TJ, Zoncu R, Bassik MC, Nomura DK, Dixon SJ, Olzmann JA (2019) The CoQ oxidoreductase FSP1 acts parallel to GPX4 to inhibit ferroptosis. Nature 575:688-692.

Chen XB, Hu YP, Wang FJ, Wang JF, TAn WB, Yuan DP (2013) Effect of sodium selenite on ciliary neurotropic factor and its receptor in different-aged rats suffering spinal cord injury. Yingyang Xuebao 35:455-459.

Chen XB, Yuan H, Wang FJ, Tan ZX, Liu H, Chen N (2015) Protective role of selenium-enriched supplement on spinal cord injury through the up-regulation of CNTF and CNTF-Ralpha. Eur Rev Med Pharmacol Sci 19:4434-4442.

Conrad M, Friedmann Angeli JP (2015) Glutathione peroxidase 4 (Gpx4) and ferroptosis: what's so special about it? Mol Cell Oncol 2:e995047.

Dixon SJ, Stockwell BR (2019) The hallmarks of ferroptosis. Annu Rev Cancer Biol 3:35-54.

Dixon SJ, Lemberg KM, Lamprecht MR, Skouta R, Zaitsev EM, Gleason CE, Patel DN, Bauer AJ, Cantley AM, Yang WS, Morrison B, 3rd, Stockwell BR (2012) Ferroptosis: an iron-dependent form of nonapoptotic cell death. Cell 149:1060-1072.

Doll S, Proneth B, Tyurina YY, Panzilius E, Kobayashi S, Ingold I, Irmler M, Beckers J, Aichler M, Walch A, Prokisch H, Trümbach D, Mao G, Qu F, Bayir H, Füllekrug J, Scheel CH, Wurst W, Schick JA, Kagan VE, et al. (2017) ACSL4 dictates ferroptosis sensitivity by shaping cellular lipid composition. Nat Chem Biol 13:91-98.

Doll S, Freitas FP, Shah R, Aldrovandi M, da Silva MC, Ingold I, Goya Grocin A, Xavier da Silva TN, Panzilius E, Scheel CH, Mourão A, Buday K, Sato M, Wanninger J, Vignane T, Mohana V, Rehberg M, Flatley A, Schepers A, Kurz A, et al. (2019) FSP1 is a glutathione-independent ferroptosis suppressor. Nature 575:693-698.

Dolma S, Lessnick SL, Hahn WC, Stockwell BR (2003) Identification of genotype-selective antitumor agents using synthetic lethal chemical screening in engineered human tumor cells. Cancer Cell 3:285-296.

Duan W, Zhang YP, Hou Z, Huang C, Zhu H, Zhang CQ, Yin Q (2016) Novel insights into NeuN: from neuronal marker to splicing regulator. Mol Neurobiol 53:1637-1647.

Eng LF, Ghirnikar RS, Lee YL (2000) Glial fibrillary acidic protein: GFAP-thirty-one years (1969-2000). Neurochem Res 25:1439-1451.

Friedmann Angeli JP, Conrad M (2018) Selenium and GPX4, a vital symbiosis. Free Radic Biol Med 127:153-159.

Gao H, You Y, Zhang G, Zhao F, Sha Z, Shen Y (2013) The use of fiber-reinforced scaffolds cocultured with Schwann cells and vascular endothelial cells to repair rabbit sciatic nerve defect with vascularization. Biomed Res Int 2013:362918.

Hassannia B, Vandenabeele P, Vanden Berghe T (2019) Targeting ferroptosis to iron out cancer. Cancer Cell 35:830-849.

Hu AM, Li JJ, Sun W, Yang DG, Yang ML, Du LJ, Gu R, Gao F, Li J, Chu HY, Zhang X, Gao LJ (2015) Myelotomy reduces spinal cord edema and inhibits aquaporin-4 and aquaporin-9 expression in rats with spinal cord injury. Spinal Cord 53:98-102.

Ingold I, Berndt C, Schmitt S, Doll S, Poschmann G, Roveri A, Peng X, Freitas FP, Aichler M, Jastroch M, Ursini F, Arnér ESJ, Fradejas-Villar N, Schweizer U, Zischka H, Angeli JPF, Conrad M (2017) 10- Selenium utilization by GPX4 was an evolutionary requirement to prevent hydroperoxide-induced ferroptosis. Free Radical Biol Med 112:24.

Ji X, Qian J, Rahman SMJ, Siska PJ, Zou Y, Harris BK, Hoeksema MD, Trenary IA, Heidi C, Eisenberg R, Rathmell JC, Young JD, Massion PP (2018) xCT (SLC7A11)-mediated metabolic reprogramming promotes non-small cell lung cancer progression. Oncogene 37:5007-5019.

Kagan VE, Mao G, Qu F, Angeli JP, Doll S, Croix CS, Dar HH, Liu B, Tyurin VA, Ritov VB, Kapralov AA, Amoscato AA, Jiang J, Anthonymuthu T, Mohammadyani D, Yang Q, Proneth B, Klein-Seetharaman J, Watkins S, Bahar I, et al. (2017) Oxidized arachidonic and adrenic PEs navigate cells to ferroptosis. Nat Chem Biol 13:81-90.

Kenny EM, Fidan E, Yang Q, Anthonymuthu TS, New LA, Meyer EA, Wang H, Kochanek PM, Dixon CE, Kagan VE, Bayir H (2019) Ferroptosis contributes to neuronal death and functional outcome after traumatic brain injury. Crit Care Med 47:410-418.

Kwon MY, Park E, Lee SJ, Chung SW (2015) Heme oxygenase-1 accelerates erastin-induced ferroptotic cell death. Oncotarget 6:24393-24403.

Livak KJ, Schmittgen TD (2001) Analysis of relative gene expression data using real-time quantitative PCR and the 2(-Delta Delta C(T)) Method. Methods 25:402-408.

Min Z, Guo Y, Sun M, Hussain S, Zhao Y, Guo D, Huang H, Heng L, Zhang F, Ning Q, Han Y, Xu P, Zhong N, Sun J, Lu S (2018) Selenium-sensitive miRNA-181a-5p targeting SBP2 regulates selenoproteins expression in cartilage. J Cell Mol Med 22:5888-5898.

Mourelo Fariña M, Salvador de la Barrera S, Montoto Marqués A, Ferreiro Velasco ME, Galeiras Vázquez R (2017) Update on traumatic acute spinal cord injury. Part 2. Med Intensiva 41:306-315.

Müller HW, Seifert W (1982) 2',3'-Cyclic nucleotide 3'-phosphodiesterase (CNPase) activity in cultured nerve cell lines from central nervous system: comparison of proliferating and resting growth states and cell cycle-dependent activity changes. Cell Mol Neurobiol 2:227-239.

No authors listed (2016) Spinal cord injury (SCI) facts and figures at a glance. J Spinal Cord Med 39:243-244.

Nottingham SA, Springer JE (2003) Temporal and spatial distribution of activated caspase-3 after subdural kainic acid infusions in rat spinal cord. J Comp Neurol 464:463-471.

Qin C, Liu CB, Yang DG, Gao F, Zhang X, Zhang C, Du LJ, Yang ML, Li JJ (2018) Circular RNA expression alteration and bioinformatics analysis in rats after traumatic spinal cord injury. Front Mol Neurosci 11:497.

Sato M, Kusumi R, Hamashima S, Kobayashi S, Sasaki S, Komiyama Y, Izumikawa T, Conrad M, Bannai S, Sato H (2018) The ferroptosis inducer erastin irreversibly inhibits system x(c)- and synergizes with cisplatin to increase cisplatin's cytotoxicity in cancer cells. Sci Rep 8:968.

Seibt TM, Proneth B, Conrad M (2019) Role of GPX4 in ferroptosis and its pharmacological implication. Free Radic Biol Med 133:144-152.

Seiler A, Schneider M, Förster H, Roth S, Wirth EK, Culmsee C, Plesnila N, Kremmer E, Rådmark O, Wurst W, Bornkamm GW, Schweizer U, Conrad M (2008) Glutathione peroxidase 4 senses and translates oxidative stress into 12/15-lipoxygenase dependent- and AIF-mediated cell death. Cell Metab 8:237-248.

Shi Z, Yuan S, Shi L, Li J, Ning G, Kong X, Feng S (2021) Programmed cell death in spinal cord injury pathogenesis and therapy. Cell Prolif 54:e12992.

Touat-Hamici Z, Legrain Y, Bulteau AL, Chavatte L (2014) Selective up-regulation of human selenoproteins in response to oxidative stress. J Biol Chem 289:14750-14761.

Wang J, Chen Y, Chen L, Duan Y, Kuang X, Peng Z, Li C, Li Y, Xiao Y, Jin H, Tan Q, Zhang S, Zhu B, Tang Y (2020) EGCG modulates PKD1 and ferroptosis to promote recovery in ST rats. Transl Neurosci 11:173-181.

Warner GJ, Berry MJ, Moustafa ME, Carlson BA, Hatfield DL, Faust JR (2000) Inhibition of selenoprotein synthesis by selenocysteine tRNA[Ser]Sec lacking isopentenyladenosine. J Biol Chem 275:28110-28119.

Wenzel SE, Tyurina YY, Zhao J, St Croix CM, Dar HH, Mao G, Tyurin VA, Anthonymuthu TS, Kapralov AA, Amoscato AA, Mikulska-Ruminska K, Shrivastava IH, Kenny EM, Yang Q, Rosenbaum JC, Sparvero LJ, Emlet DR, Wen X, Minami Y, Qu F, et al. (2017) PEBP1 wardens ferroptosis by enabling lipoxygenase generation of lipid death signals. Cell 171:628-641.e26.

Wirth EK, Conrad M, Winterer J, Wozny C, Carlson BA, Roth S, Schmitz D, Bornkamm GW, Coppola V, Tessarollo L, Schomburg L, Köhrle J, Hatfield DL, Schweizer U (2010) Neuronal selenoprotein expression is required for interneuron development and prevents seizures and neurodegeneration. FASEB J 24:844-852.

Wu Y, Song J, Wang Y, Wang X, Culmsee C, Zhu C (2019) The potential role of ferroptosis in neonatal brain injury. Front Neurosci 13:115.

Xie BS, Wang YQ, Lin Y, Mao Q, Feng JF, Gao GY, Jiang JY (2019) Inhibition of ferroptosis attenuates tissue damage and improves long-term outcomes after traumatic brain injury in mice. CNS Neurosci Ther 25:465-475.

Xie Y, Hou W, Song X, Yu Y, Huang J, Sun X, Kang R, Tang D (2016) Ferroptosis: process and function. Cell Death Differ 23:369-379.

Yang WS, Stockwell BR (2008) Synthetic lethal screening identifies compounds activating iron-dependent, nonapoptotic cell death in oncogenic-RAS-harboring cancer cells. Chem Biol 15:234-245.

Yang WS, Kim KJ, Gaschler MM, Patel M, Shchepinov MS, Stockwell BR (2016) Peroxidation of polyunsaturated fatty acids by lipoxygenases drives ferroptosis. Proc Natl Acad Sci U S A 113:E4966-4975.

Yang WS, SriRamaratnam R, Welsch ME, Shimada K, Skouta R, Viswanathan VS, Cheah JH, Clemons PA, Shamji AF, Clish CB, Brown LM, Girotti AW, Cornish VW, Schreiber SL, Stockwell BR (2014) Regulation of ferroptotic cancer cell death by GPX4. Cell 156:317-331.

Yao X, Zhang Y, Hao J, Duan HQ, Zhao CX, Sun C, Li B, Fan BY, Wang X, Li WX, Fu XH, Hu Y, Liu C, Kong XH, Feng SQ (2019) Deferoxamine promotes recovery of traumatic spinal cord injury by inhibiting ferroptosis. Neural Regen Res 14:532-541.

Yeo JE, Kim JH, Kang SK (2008) Selenium attenuates ROS-mediated apoptotic cell death of injured spinal cord through prevention of mitochondria dysfunction; in vitro and in vivo study. Cell Physiol Biochem 21:225-238.

Zhang Y, Sun C, Zhao C, Hao J, Zhang Y, Fan B, Li B, Duan H, Liu C, Kong X, Wu P, Yao X, Feng S (2019) Ferroptosis inhibitor SRS 16-86 attenuates ferroptosis and promotes functional recovery in contusion spinal cord injury. Brain Res 1706:48-57.

Zhang Z, Wu Y, Yuan S, Zhang P, Zhang J, Li H, Li X, Shen H, Wang Z, Chen G (2018) Glutathione peroxidase 4 participates in secondary brain injury through mediating ferroptosis in a rat model of intracerebral hemorrhage. Brain Res 1701:112-125.

Zhou H, Yin C, Zhang Z, Tang H, Shen W, Zha X, Gao M, Sun J, Xu X, Chen Q (2020) Proanthocyanidin promotes functional recovery of spinal cord injury via inhibiting ferroptosis. J Chem Neuroanat 107:101807.

Zille M, Karuppagounder SS, Chen Y, Gough PJ, Bertin J, Finger J, Milner TA, Jonas EA, Ratan RR (2017) Neuronal death after hemorrhagic stroke in vitro and in vivo shares features of ferroptosis and necroptosis. Stroke 48:1033-1043.

C-Editor: Zhao M; S-Editors: Yu J, Li CH; L-Editors: Zunino S, Yu J, Song LP; T-Editor: Jia Y